Gold Clusters

DOI: 10.1002/anie.201410161

Structure Determination of $[Au_{18}(SR)_{14}]$**

Anindita Das, Chong Liu, Hee Young Byun, Katsuyuki Nobusada, Shuo Zhao, Nathaniel Rosi, and Rongchao Jin**

Abstract: *Unravelling the atomic structures of small gold clusters is the key to understanding the origin of metallic bonds and the nucleation of clusters from organometallic precursors. Herein we report the X-ray crystal structure of a charge-neutral $[Au_{18}(SC_6H_{11})_{14}]$ cluster. This structure exhibits an unprecedented bi-octahedral (or hexagonal close packing) Au_9 kernel protected by staple-like motifs including one tetramer, one dimer, and three monomers. Until the present, the $[Au_{18}(SC_6H_{11})_{14}]$ cluster is the smallest crystallographically characterized gold cluster protected by thiolates and provides important insight into the structural evolution with size. Theoretical calculations indicate charge transfer from surface to kernel for the HOMO–LUMO transition.*

Ligand-protected gold nanoclusters lie at the interface between organo-gold complexes (e.g. $[Au^I(SR)]$) and plasmonic gold nanoparticles.[1–9] The distinct valence state of the metal atoms give a "metalloid" nature to such nanoclusters.[10] Understanding the nucleation of $[Au^I(SR)]$ complexes into clusters (i.e. $[Au_n(SR)_m]$, where $n > m$) is of critical importance for mapping out the growth pattern. To achieve that, discrete-sized clusters should be made and their structures solved by X-ray crystallography. In the case of thiolate-protected $[Au_n(SR)_m]$ nanoclusters, following the initial efforts of structural elucidation of $[Au_{25}(SC_2H_4Ph)_{18}]$, $[Au_{38}(SC_2H_4Ph)_{24}]$, and $[Au_{102}(SPh\text{-}p\text{-}COOH)_{44}]$ (see Review Ref. [1]), several new crystal structures toward the smaller end ($n < 25$) have been attained recently,[11,12] including $[Au_{24}(SCH_2Ph\text{-}tBu)_{20}]$ featuring a Au_8 kernel protected by four tetrameric $Au_4(SR)_5$ staples, $[Au_{23}(SC_6H_{11})_{16}]$ with a Au_{15} kernel protected by various surface motifs, and $[Au_{20}(SPh\text{-}tBu)_{16}]$ exhibiting a Au_7 kernel and an unprecedented $Au_8(SR)_8$ macrocyclic ring as one of the surface-protecting motifs.

Crystallization of even smaller clusters (e.g. $n < 20$), however, has not been successful, although small $[Au_n(SR)_m]$ clusters were reported a decade ago.[13,14] Negishi et al. first isolated $[Au_{10-12}(SG)_{10-12}]$ complexes and clusters including $[Au_{15}(SG)_{13}]$, $[Au_{18}(SG)_{14}]$, where SG is deprotonated glutathione.[13] In recent work, Hamouda et al. also observed similar sizes together with charge-neutral $[Au_{18}(SG)_{14}]$ and $[Au_{20}(SG)_{16}]$ clusters.[15] Pradeep and coworkers reported a one-step, slow reduction route for the synthesis of $[Au_{18}(SG)_{14}]$ and further studied the photoluminescence.[16] Yao et al. recently devised a pH value-controlled method for one-pot synthesis of $[Au_{15}(SG)_{13}]$ and $[Au_{18}(SG)_{14}]$ without the need of isolation.[17] The catalytic application of $[Au_{15}(SG)_{13}]$ and $[Au_{18}(SG)_{14}]$ has been reported.[18] In theoretical work, Tlahuice and Garzon predicted the $[Au_{18}(SR)_{14}]$ structure to be a prolate bitetrahedral Au_8 core capped by two dimers (-SR-Au-SR-Au-SR-) and two trimers (-SR-Au-SR-Au-SR-Au-SR-).[19] Despite the identification of $[Au_{18}(SG)_{14}]$ a decade ago and subsequent extensive work, crystallization of $[Au_{18}(SG)_{14}]$ has not been successful thus far. After years of trials, we realized that the barrier could be the SG ligand, since structure determinations on $[Au_n(SR)_m]$ with organic soluble thiolates have been quite successful.[1,20,21] This motivated us to devise a new synthetic strategy to obtain thiolate-protected Au_{18} clusters that are soluble in organic solvents for the realization of crystallization.

In this work, we have successfully devised a facile synthesis for a cyclohexanethiolate-protected Au_{18} cluster and determined its structure by X-ray crystallography. This charge-neutral cluster features a face-fused Au_9 bi-octahedral (or hexagonal close packing) kernel, and the surface protecting motifs include one $Au_4(SR)_5$ tetramer, one $Au_2(SR)_3$ dimer, and three $Au(SR)_2$ monomers.

The $[Au_{18}(SC_6H_{11})_{14}]$ nanoclusters were synthesized in a one-pot reaction at room temperature by a kinetically controlled approach[22] (see Experimental Section for details). This synthetic route yielded pure $[Au_{18}(SC_6H_{11})_{14}]$ nanoclusters with the optical absorption spectrum closely resembling that of $[Au_{18}(SG)_{14}]$.[13,14] Recrystallization and single crystal growth of the nanoclusters were performed by vapor diffusion of pentane into a concentrated solution of the nanoclusters in CH_2Cl_2 for 1–2 days.

The structure (Figure 1) of $[Au_{18}(SC_6H_{11})_{14}]^0$ was solved by single-crystal X-ray crystallography. The structure is

[*] A. Das, H. Y. Byun,[+] S. Zhao, Prof. R. Jin
Department of Chemistry
Carnegie Mellon University
Pittsburgh, PA 15213 (USA)
E-mail: rongchao@andrew.cmu.edu
C. Liu,[+] Prof. N. L. Rosi
Department of Chemistry, University of Pittsburgh
Pittsburgh, PA 15213 (USA)
Prof. K. Nobusada
Department of Theoretical and Computational Molecular Science, Institute for Molecular Science
Myodaiji, Okazaki, 444-8585 (Japan)
and
Elements Strategy Initiative for Catalysts and Batteries (ESICB), Kyoto University
Katsura, Kyoto 615-8520 (Japan)
E-mail: nobusada@ims.ac.jp
[+] These authors contributed equally to this work.

[**] R.J. acknowledges financial support from the U.S. Department of Energy-Office of Basic Energy Sciences, grant DE-FG02-12ER16354. K.N. acknowledges financial support from MEXT (Japan), Grant-in-Aid No. 25288012, and from ESICB. We thank Zhongrui Zhou for assistance in ESI-MS analysis.
Supporting information for this article is available on the WWW under http://dx.doi.org/10.1002/anie.201410161.

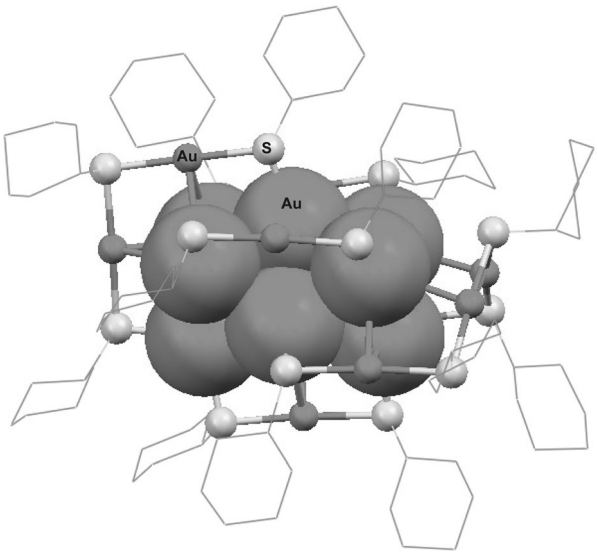

Figure 1. X-ray structure of the $[Au_{18}(SC_6H_{11})_{14}]^0$ nanocluster. The Au atoms are dark gray, sulfur atoms light gray, cyclohexyl in wireframe, all H atoms are omitted for clarity.[39]

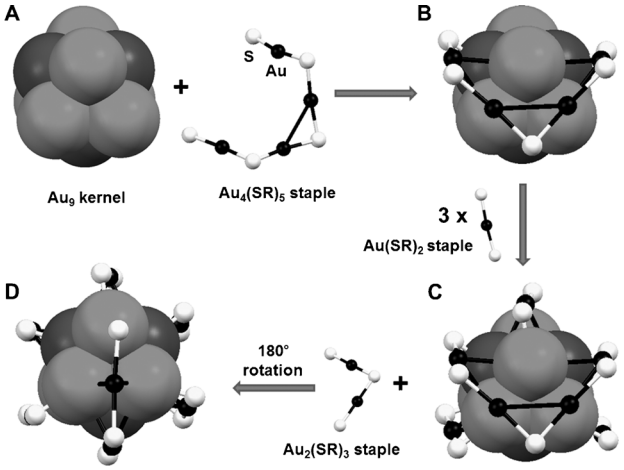

Figure 3. Anatomy of the $[Au_{18}(SC_6H_{11})_{14}]^0$ nanocluster, starting with the bi-octahedral Au_9 kernel (A), to which one tetrameric staple motif is added giving (B), followed by addition of three monomeric staples to give (C), and finally addition of a dimeric staple motif yields the complete structure $[Au_{18}(SC_6H_{11})_{14}]$ (D). (large spheres = Au in the kernel; dark small spheres = Au in the staples; light gray spheres = S; carbon tails of thiolates are omitted for clarity).

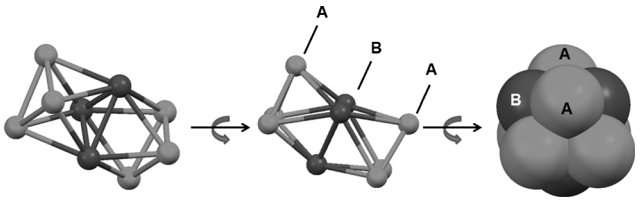

Figure 2. The Au_9 bi-octahedral kernel of the $[Au_{18}(SC_6H_{11})_{14}]^0$ nanocluster with the shared Au_3 face highlighted in dark gray. The Au_9 kernel can also be viewed as three Au_3 layers (ABA) arranged in a hcp fashion. The right panel shows the Au_9 kernel in space-filling model.[39]

composed of a face-fused bi-octahedral Au_9 kernel (Figure 2a), where two Au_6 octahedra are fused together by sharing a common Au_3 face. The Au–Au bonds in the Au_9 kernel range from 2.67 to 3.00 Å (average: 2.82 Å), which is comparable to the Au–Au distance (2.88 Å) in bulk gold. Alternatively, the face-fused bi-octahedral Au_9 kernel may be viewed as three layers of Au_3 planes arranged in a hexagonal close-packing (hcp) fashion (Figure 2, labeled ABA layers). Of note, the Au–Au bonds within each of the three Au_3 planes range from 2.67 to 2.81 Å and are considerably shorter than the Au–Au bonds between the layers (ranging from 2.78 to 3.00 Å). It is worth comparing with the $[Al_{12}\{N(SiMe_3)_2\}_8]^-$ structure.[10b] While Al and Au clusters bear some similarities[10a] (e.g. both being face-centered cubic (fcc) and having similar metal–metal distances, Al–Al: 2.86 Å and Au–Au: 2.88 Å), the $[Al_{12}\{N(SiMe_3)_2\}_8]^-$ cluster exhibits a central Al_9 unit of fcc structure, whereas $[Au_{18}(SR)_{14}]$ has a hcp Au_9 kernel.

The hcp-layered Au_9 kernel is encapsulated by one $Au_4(SR)_5$ tetramer, one $Au_2(SR)_3$ dimer, and three $Au(SR)_2$ monomers. Specifically, the two sulfur ends of the $Au_4(SR)_5$ tetrameric staple are bonded with two Au atoms of the middle Au_3 layer of the Au_9 kernel and the tetramer spans across the front Au_3 face (Figure 3B). The three $Au(SR)_2$ monomers bridge Au atoms of the front and back Au_3 layers (Figure 3C) and are symmetrically distributed. Finally, a dimeric staple extends from the middle Au_3 layer to the back Au_3 face (rotated 180° to the front, Figure 3D). Interestingly, the $Au_4(SR)_5$ staple is skewed, unlike the tetramer found in the $[Au_{24}(SCH_2Ph\text{-}tBu)_{20}]^0$ structure (Supporting Information, Figure S1),[11a] and it appears to be caused by the relatively stronger interaction (3.16 Å) between the two Au atoms of the tetramer (see Figure S1(A)), as opposed to commonly seen Au–Au distances in staple motifs of gold clusters (over 3.3 Å, see Table S1). In addition, the Au atoms in all three types of staple motifs residing on the Au_9 kernel have strong contacts with the Au atoms of the kernel (Au–Au distances ranging from 2.88–3.58 Å, average 3.23 Å), giving rise to a compact cluster structure. The cluster is non-chiral, as there is a symmetry plane in the $[Au_{18}S_{14}]$ framework, along the plane of the dimeric staple (Figure 3D); this symmetry plane also cuts the tetrameric staple into left and right symmetric halves (Figure 3C). Note that Tlahuice and Garzon theoretically predicted the structure of $[Au_{18}(SR)_{14}]$ to be composed of a bi-tetrahedral Au_8 kernel protected by two dimers and two trimers.[19] This predicted structure does not match with our experimental one.

No counterion was found in the unit cell of $[Au_{18}(SC_6H_{11})_{14}]$ crystals, and the charge neutrality of the cluster was further confirmed by electrospray ionization mass spectrometric (ESI-MS) analysis; no signals was observed in both positive and negative mode analyses prior to the addition of cesium acetate (CsOAc). With CsOAc, the clusters formed a positively charged mono-Cs^+ adduct which was detected in positive mode ESI-MS (Figure S2). An intense peak was observed at m/z 5291.12, which corresponds to $[Au_{18}(SC_6H_{11})_{14}\text{–}Cs]^+$ adduct. The isotope pattern further revealed the isotope peak spacing to be unity,

confirming the ionized cluster to be +1 charged. After subtracting one Cs^+, the cluster mass is determined to be 5158.22, which is in excellent agreement with the theoretical mass (5158.42, deviation 0.2 Da).

With regard to the optical properties of $[Au_{18}(SC_6H_{11})_{14}]$, the UV/Vis spectrum exhibits prominent bands at 450, 570, and 630 nm (Figure 4), and the optical energy gap (E_g) is

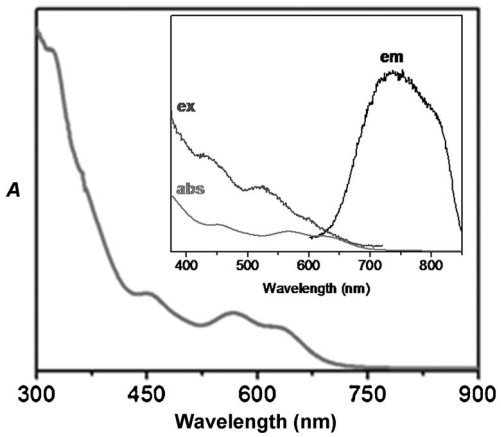

Figure 4. UV/Vis absorption spectrum of the $[Au_{18}(SC_6H_{11})_{14}]^0$ nanocluster. Inset: excitation, emission, and UV/Vis absorption profiles.

determined to be 1.7 eV by extrapolating the absorbance to zero. Electrochemical measurements gave the first reduction peak at −0.95 V (vs. Ag/AgCl) and the first oxidation at +0.87 V (Figure S3). By extrapolating the peaks to the baseline we obtain the electrochemical gap energy of approximately 1.66 eV, in agreement with the optically measured gap of 1.7 eV. The absorption spectrum closely matches with that of water-soluble $[Au_{18}(SG)_{14}]$ reported by Negishi et al.,[14] indicating that both $[Au_{18}(SC_6H_{11})_{14}]$ and $[Au_{18}(SG)_{14}]$ clusters share the same structure. Photoluminescence measurements revealed that the $[Au_{18}(SC_6H_{11})_{14}]$ cluster gives rise to red emission centered at around 735 nm (excitation: 450 nm). The corresponding excitation spectrum exhibits multiple bands resembling the absorption spectrum (Figure 4, inset). The quantum yield (QY) of $[Au_{18}(SC_6H_{11})_{14}]$ was measured to be approximately 0.05% using the well-studied $[Au_{25}(SG)_{18}]^-$ as the reference (QY: 0.2%).[23,24] We note that the quantum yield of the SG-protected clusters is typically 10–100 times higher than that of the organic-thiolate-protected counterpart owing to the surface ligand effect.[24] The origin of the luminescence is largely ascribed to the surface effect,[24,25] while the inner metal core plays a less-important role.

To gain insight into the electronic and optical absorption properties of the cluster, we carried out density functional theory (DFT) calculations. The simulated optical absorption spectrum is shown in Figure 5A, in which the lowest energy peak arises from the HOMO–LUMO electronic transition. Unlike other nanoclusters,[1] an interesting feature of $[Au_{18}(SC_6H_{11})_{14}]$ lies in that the HOMO extends over to the $Au_4(SR)_5$ staple (Figure 5B), and indeed all the four gold atoms and five sulfur atoms of this extended staple are involved in the HOMO. The LUMO, on the other hand, is over the three layers of the Au_9 kernel. Thus, the HOMO–LUMO transition manifests charge transfer from the $Au_4(SR)_5$ staple to the Au_9 kernel, a feature not found in other nanoclusters.[1] The simulated optical absorption spectrum reproduces well the experimental observation, except for a small redshift (ca. 0.22 eV) of the computed result. The DFT results also verify the tetrameric gold-thiolate motif assigned in the above structural anatomy.

It is worth commenting on the structures of the clusters close in size.[11,12,19,26–31] Previous studies (both experiment and theory) have predicted a reduction in gold-kernel size with decreasing size of the cluster (Table 1), and a small kernel encapsulated by extended staple motifs is believed to stabilize the cluster structure.[19,26–31] However, upon careful analysis of the gold cores in experimentally determined crystal structures

Table 1: Small $[Au_n(SR)_m]$ clusters ($n<25$) and their Au kernels.

$[Au_n(SR)_m]$	Au kernel (experiment)	Au kernel (theory)
$[Au_{15}(SR)_{13}]$	–	Au_4
$[Au_{18}(SR)_{14}]$	Au_9	Au_8
$[Au_{20}(SR)_{16}]$	Au_7	Au_8
$[Au_{22}(SR)_{18}]$	–	Au_8
$[Au_{23}(SR)_{16}]$	Au_{15}	–
$[Au_{24}(SR)_{20}]$	Au_8 (different configuration from theory)	Au_8

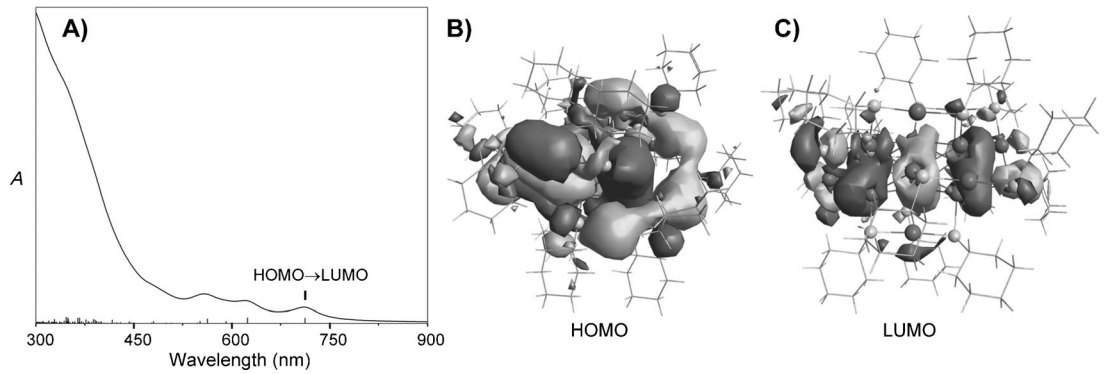

Figure 5. A) Simulated absorption spectrum of the $[Au_{18}(SC_6H_{11})_{14}]^0$ nanocluster; B) HOMO distribution; C) LUMO distribution. The stick pattern under the absorption curve in (A) indicates the individual electronic transitions.

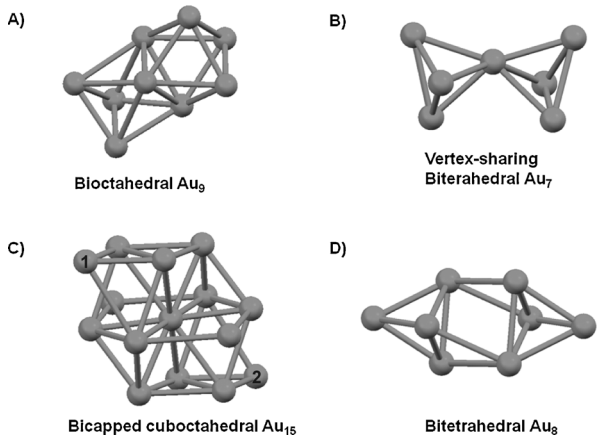

Figure 6. Experimentally determined gold kernels of A) $[Au_{18}(SC_6H_{11})_{14}]$, B) $[Au_{20}(SPh\text{-}tBu)_{16}]$, C) $[Au_{23}(SC_6H_{11})_{16}]$ (the labels 1 and 2 indicate the two capping Au atoms on the Au_{13} cuboctahedron), and D) $[Au_{24}(SCH_2Ph\text{-}tBu)_{16}]$.

of small $[Au_n(SR)_m]$ clusters (where, $n < 25$),[11,12] we find that the predicted trend does not hold (Table 1 and Figure 6). This indicates that the structures of clusters at the smaller end are much more diverse than previously thought.

The successful determination of the $[Au_{18}(SR)_{14}]$ structure leaves that of the smallest, $[Au_{15}(SR)_{13}]$, to be solved in future efforts. Between $[Au^I(SR)]_{10-12}$ complexes and $[Au_{15}(SR)_{13}]$, no cluster sizes have been found. In contrast, phosphine-protected gold clusters ranging continuously from Au_2 to Au_{14} have been identified.[3,4,6,32–35] The four-electron (4e) family of $[Au_n(SR)_m]$ nanoclusters include $[Au_{18}(SR)_{14}]$, $[Au_{20}(SR)_{16}]$, and $[Au_{24}(SR)_{20}]$,[11a] as well as the SePh protected counterparts.[21a,36] From Au_{24} to Au_{20}, a decrease in Au-kernel size is seen from the face-joined bi-tetrahedral Au_8^{4+} in $[Au_{24}(SR)_{20}]$ to vertex-shared bi-tetrahedral Au_7^{3+} in $[Au_{20}(SR)_{16}]$.[11a,12] However, $[Au_{18}(SR)_{14}]$ does not follow the shrinking trend and, instead, a larger Au_9^{5+} kernel is observed in $[Au_{18}(SR)_{14}]$. This Au_9^{5+} kernel comprises three layers of gold atoms and can be viewed as two Au_6 octahedral units sharing a common face, in contrast with the linking of Au_4 tetrahedra in the larger 4e clusters.[11a,12,21a] With respect to the phosphine-protected Au_{20} and Au_{24} clusters, the gold kernels are based on icosahedral or incomplete icosahedral units.[5,37] A phosphine-protected 4e $[Au_7]^{3+}$ cluster has also been reported,[38] which exhibits a structure of octahedral Au_6 core plus one atom and fills the gap between the $[Au_6]^{2+}$ and $[Au_8]^{4+}$ clusters with "core + two" structures.[6] The striking differences between $[Au_n(SR)_m]$ and the gold-phosphine system reflects the Au–SR and Au–PR_3 bonding differences.

In summary, we have devised a facile one-pot synthesis for obtaining molecularly pure $[Au_{18}(SC_6H_{11})_{14}]$ and successfully solved its structure. This cluster constitutes the hitherto smallest crystallographically characterized $[Au_n(SR)_m]$ cluster. Theoretical simulations reveal that the HOMO–LUMO electronic transition exhibits charge transfer from the surface to the kernel, a feature not found in other reported nanoclusters. The observation of a face-fused Au_9 bi-octahedral (or hexagonal close packing) kernel in a small $[Au_{18}(SC_6H_{11})_{14}]$ cluster is remarkable and it offers insights into nucleation and size evolution of gold clusters.[40]

Experimental Section

$[Au_{18}(SC_6H_{11})_{14}]$: In a typical reaction, $HAuCl_4 \cdot 3H_2O$ (0.2 mmol, 78.8 mg, dissolved in 0.5 mL ethanol) was added to a CH_2Cl_2 (10 mL) solution of tetraoctylammonium bromide (TOAB, 0.232 mmol, 127 mg). After vigorously stirring for 15 min, the solution changed from yellow to dark reddish orange. Then, excess 1-cyclohexanethiol (125 μL, neat) was added to the mixture at room temperature. The reddish orange solution turned colorless in 15–20 min indicating the conversion of Au^{III} into Au^I complexes. Then, $NaBH_4$ (0.5 mmol, 19 mg dissolved freshly in 1.5 mL of ethanol) was added drop-wise to the solution under vigorous stirring. The solution slowly turned green, indicating the formation of clusters (identified to be $[Au_{18}(SC_6H_{11})_{14}]$). The mixture was further allowed to react for 4–5 h under stirring, after which it was centrifuged to remove insoluble Au^I-polymers. The supernatant solution was evaporated to dryness under rotary evaporation and the product was washed several times with methanol to remove excess reactants. The purified nanocluster product was then extracted with CH_2Cl_2 and recrystallized by vapor diffusion of pentane into the CH_2Cl_2 solution of the cluster for 1–2 days. This step was repeated 2–3 times to obtain high quality single crystals of the nanocluster for X-ray crystallography. Details of the X-ray analysis, electrochemical and mass spectrometric analyses, optical spectroscopic measurements, and density functional theory (DFT) calculations are provided in the Supporting Information.

Received: October 16, 2014
Revised: December 7, 2014
Published online: January 23, 2015

Keywords: gold · nanoclusters · structure elucidation · sulfur ligands

[1] H. Qian, M. Zhu, Z. Wu, R. Jin, *Acc. Chem. Res.* **2012**, *45*, 1470–1479.
[2] G. Schmid, *Chem. Rev.* **1992**, *92*, 1709–1727.
[3] Z. Lin, R. P. F. Kanters, D. M. P. Mingos, *Inorg. Chem.* **1991**, *30*, 91–95.
[4] B. S. Gutrath, I. M. Oppel, O. Presly, I. Beljakov, V. Meded, W. Wenzel, U. Simon, *Angew. Chem. Int. Ed.* **2013**, *52*, 3529–3532; *Angew. Chem.* **2013**, *125*, 3614–3617.
[5] a) X.-K. Wan, S.-F. Yuan, Z.-W. Lin, Q.-M. Wang, *Angew. Chem. Int. Ed.* **2014**, *53*, 2923–2926; *Angew. Chem.* **2014**, *126*, 2967–2970; b) X.-K. Wan, Z.-W. Lin, Q.-M. Wang, *J. Am. Chem. Soc.* **2012**, *134*, 14750–14752.
[6] N. Kobayashi, Y. Kamei, Y. Shichibu, K. Konishi, *J. Am. Chem. Soc.* **2013**, *135*, 16078–16081.
[7] J. Chen, Q.-F. Zhang, T. A. Bonaccorso, P. G. Williard, L.-S. Wang, *J. Am. Chem. Soc.* **2014**, *136*, 92–95.
[8] a) S. Knoppe, T. Bürgi, *Acc. Chem. Res.* **2014**, *47*, 1318–1326; b) H. Yao, *J. Phys. Chem. Lett.* **2012**, *3*, 1701–1706.
[9] H. Yang, Y. Wang, J. Yan, X. Chen, X. Zhang, H. Häkkinen, N. Zheng, *J. Am. Chem. Soc.* **2014**, *136*, 7197–7200.
[10] a) H. Schnöckel, A. Schnepf, R. L. Whetten, C. Schenk, P. Henke, *Z. Anorg. Allg. Chem.* **2011**, *637*, 15–23; b) A. Purath, R. Köppe, H. Schnöckel, *Chem. Commun.* **1999**, 1933–1934.
[11] a) A. Das, T. Li, G. Li, K. Nobusada, C. Zeng, N. L. Rosi, R. Jin, *Nanoscale* **2014**, *6*, 6458–6462; b) A. Das, T. Li, K. Nobusada, C. Zeng, N. L. Rosi, R. Jin, *J. Am. Chem. Soc.* **2013**, *135*, 18264–18267.
[12] C. Zeng, C. Liu, Y. Chen, N. L. Rosi, R. Jin, *J. Am. Chem. Soc.* **2014**, *136*, 11922–11925.
[13] Y. Negishi, Y. Takasugi, S. Sato, H. Yao, K. Kimura, T. Tsukuda, *J. Am. Chem. Soc.* **2004**, *126*, 6518–6519.
[14] Y. Negishi, K. Nobusada, T. Tsukuda, *J. Am. Chem. Soc.* **2005**, *127*, 5261–5270.

[15] R. Hamouda, F. Bertorelle, D. Rayane, R. Antoine, M. Broyer, P. Dugourd, *Int. J. Mass Spectrom.* **2013**, *335*, 1.
[16] a) A. Ghosh, T. Udayabhaskararao, T. Pradeep, *J. Phys. Chem. Lett.* **2012**, *3*, 1997 – 2002; b) E. S. Shibu, T. Pradeep, *Chem. Mater.* **2011**, *23*, 989 – 999.
[17] Q. Yao, Y. Yu, X. Yuan, Y. Yu, J. Xie, J. Y. Lee, *Small* **2013**, *9*, 2696 – 2701.
[18] G. Li, D.-e. Jiang, S. Kumar, Y. Chen, R. Jin, *ACS Catal.* **2014**, *4*, 2463 – 2469.
[19] A. Tlahuice, I. L. Garzon, *Phys. Chem. Chem. Phys.* **2012**, *14*, 3737 – 3740.
[20] C. Zeng, H. Qian, T. Li, G. Li, N. L. Rosi, B. Yoon, R. N. Barnett, R. L. Whetten, U. Landman, R. Jin, *Angew. Chem. Int. Ed.* **2012**, *51*, 13114 – 13118; *Angew. Chem.* **2012**, *124*, 13291 – 13295.
[21] a) Y. Song, S. Wang, J. Zhang, X. Kang, S. Chen, P. Li, H. Sheng, M. Zhu, *J. Am. Chem. Soc.* **2014**, *136*, 2963 – 2965; b) D. Crasto, S. Malola, G. Brosofsky, A. Dass, H. Häkkinen, *J. Am. Chem. Soc.* **2014**, *136*, 5000 – 5005.
[22] M. Zhu, H. Qian, R. Jin, *J. Am. Chem. Soc.* **2009**, *131*, 7220 – 7221.
[23] M. A. H. Muhammed, A. K. Shaw, S. K. Pal, T. Pradeep, *J. Phys. Chem. C* **2008**, *112*, 14324 – 14330.
[24] Z. Wu, R. Jin, *Nano Lett.* **2010**, *10*, 2568 – 2573.
[25] S. Kumar, R. Jin, *Nanoscale* **2012**, *4*, 4222 – 4227.
[26] D.-e. Jiang, S. H. Overbury, S. Dai, *J. Am. Chem. Soc.* **2013**, *135*, 8786 – 8789.
[27] A. Tlahuice-Flores, M. J. Yacaman, R. L. Whetten, *Phys. Chem. Chem. Phys.* **2013**, *15*, 19557 – 19560.
[28] Y. Pei, R. Pal, C. Liu, Y. Gao, Z. Zhang, X. C. Zeng, *J. Am. Chem. Soc.* **2012**, *134*, 3015 – 3024.
[29] Y. Pei, Y. Gao, N. Shao, X. C. Zeng, *J. Am. Chem. Soc.* **2009**, *131*, 13619 – 13621.
[30] D.-e. Jiang, W. Chen, R. L. Whetten, Z. Chen, *J. Phys. Chem. C* **2009**, *113*, 16983 – 16987.
[31] Y. Yu, Z. Luo, D. M. Chevrier, D. T. Leong, P. Zhang, D.-e. Jiang, J. Xie, *J. Am. Chem. Soc.* **2014**, *136*, 1246 – 1249.
[32] D. M. P. Mingos, *Pure Appl. Chem.* **1980**, *52*, 705 – 712.
[33] Y. Kamei, Y. Shichuba, K. Konishi, *Angew. Chem. Int. Ed.* **2011**, *50*, 7442 – 7445; *Angew. Chem.* **2011**, *123*, 7580 – 7583.
[34] L. Malatesta, *Gold Bull.* **1975**, *8*, 48 – 52.
[35] J. M. Pettibone, J. W. Hudgens, *J. Phys. Chem. Lett.* **2010**, *1*, 2536 – 2540.
[36] Q. Xu, S. Wang, Z. Liu, G. Xu, X. Meng, M. Zhu, *Nanoscale* **2013**, *5*, 1176 – 1182.
[37] A. Das, T. Li, K. Nobusada, Q. Zeng, N. L. Rosi, R. Jin, *J. Am. Chem. Soc.* **2012**, *134*, 20286 – 20289.
[38] Y. Shichibu, M. Zhang, Y. Kamei, K. Konishi, *J. Am. Chem. Soc.* **2014**, *136*, 12892 – 12895.
[39] CCDC 1044239, contain the supplementary crystallographic data for this paper. These data can be obtained free of charge from The Cambridge Crystallographic Data Centre via www.ccdc.cam.ac.uk/data_request/cif.
[40] After acceptance of this manuscript we learnt of another publication reporting the crystal structure of a $[Au_{18}(SR)_{14}]$ nanocluster: S. Chen, S. Wang, J. Zhong, Y. Song, J. Zhang, H. Sheng, Y. Pei, M. Zhu, *Angew. Chem. Int. Ed.* **2015**, *54*, 3145 – 3149; *Angew. Chem.* **2015**, *127*, 3188 – 3192.

